Numerical simulations of the polariton kinetic energy distribution in GaAs quantum-well microcavity structures

V. E. Hartwell* and D. W. Snoke
Department of Physics and Astronomy, University of Pittsburgh, Pittsburgh, Pennsylvania 15260, USA
(Received 15 March 2010; revised manuscript received 9 July 2010; published 9 August 2010)

Recent experiments have shown that polaritons in microcavities behave like a Bose-Einstein condensate above a critical density threshold and at low temperature. The polaritons are not in full equilibrium, however, due to particle decay and streaming in of generated particles from high-energy states. In this paper we present a full simulation of the thermalization of polariton and exciton populations, including polariton-polariton (and exciton-exciton) scattering, phonon emission and absorption, and polariton scattering with free electrons. We find that we can obtain good fits over a wide range of polariton densities. The fits imply that the enhancement of the polariton-polariton scattering due to Bose-Einstein statistics does indeed play the major role in the particles piling up in low-energy states, which is the precursor to Bose condensation. Our fits also indicate that at low density, scattering of the polaritons with free electrons plays a more important role than polariton-phonon scattering.

DOI: 10.1103/PhysRevB.82.075307 PACS number(s): 71.36.+c, 71.35.Lk, 05.30.−d, 05.70.Ln

I. INTRODUCTION

In the past few years, there has been tremendous progress on coherent effects of polaritons in semiconductor microcavities.[1–8] (For a review of general microcavity polariton properties, see Ref. 9; for a review of condensation effects, see Ref. 10.) These particles have lifetime long enough for spontaneous coherence to arise via particle-particle scattering even under incoherent generation of the particles, but the lifetime of the particles is not extremely long compared to the scattering time. Therefore the system is not in complete equilibrium. In particular, under continuous or quasicontinuous generation, hot particles are constantly being created and stream down into the low-energy states, leading to a higher population in high-energy states than expected in equilibrium.

A general question which has been asked regarding this system is to what degree the behavior of the system is similar to a laser and to what degree it is similar to a Bose-Einstein condensate.[11] We can distinguish three different regimes. In the case of very short lifetime compared to interparticle scattering time, the system will act like an ensemble of independent oscillators, and will emit coherent light in the same way as a laser.[12] In the case of lifetime long compared to the scattering time, the system will be to all intents and purposes the same as an equilibrium Bose-Einstein condensate with number conservation. Somewhere between these two limits is a regime in which interparticle interactions play the main role in building up coherence but are not strong enough to fully equilibrate the gas. We can call this regime the "nonequilibrium Bose-Einstein condensate." This regime is evidenced by a buildup of particles in low-energy states due to collisions and spontaneous coherence in the ground state but lack of complete thermalization in high-energy states.

In this paper we show that the polariton gas in previous experiments falls in this middle regime. We use a quantum Boltzmann equation (also known as a Fokker-Planck equation) to simulate the population dynamics of the polaritons for realistic experimental parameters. We find that we can fit a large range of experimental data under steady-state and quasisteady-state conditions with reasonable estimates of the polariton-polariton scattering cross section. One feature of our model in comparison to other models is that we can simulate the entire set of polariton and excitons in one continuous, single band of energy, rather than treating the polaritons and excitons as two separate populations.

II. KINETIC MODELS FOR MICROCAVITY POLARITONS

Numerical solutions to the Boltzmann equation have been done for some time now. In general, the equation to be solved has the form,

$$\frac{\partial n_{\vec{k}}}{\partial t} = P_{\vec{k}}(t) - \frac{n_{\vec{k}}}{\tau_{\vec{k}}} + \sum_{\vec{k}'} W^{(i)}_{\vec{k}'\to\vec{k}}(t) - \sum_{\vec{k}'} W^{(i)}_{\vec{k}\to\vec{k}'}(t), \qquad (1)$$

where $n_{\vec{k}}$ is the occupation number of the state $\vec{k}$. The two terms $P_{\vec{k}}(t)$ and $-n_{\vec{k}}/\tau_{\vec{k}}$ are the pumping and recombination/loss terms, respectively, and the $W^{(i)}$'s are whatever in-scattering and out-scattering rates are to be considered. A rigorous quantum mechanical derivation of this type of equation can be found in Ref. 13, Sec. 4.8. Because the equation only involves average occupation numbers of states, it cannot treat directly the coherence in the system. However, it can show the buildup of particles in low-energy states which is the precursor for coherence in Bose-Einstein condensation.

The time scale for equilibration and onset of condensation via elastic scattering of particles in three dimensions was found by Snoke and Wolfe,[14] with subsequent work showing Bose condensation of excitons by phonon emission[15,16] and equilibration of an electron gas.[17] In Ref. 14, it was shown that in the case of an isotropic gas, the 12-dimensional integrals for the scattering rates can be reduced analytically down to just an integral over two energies; a computer can then be used to numerically calculate the evolution of the distribution function by iteration. Numerous groups have applied similar algorithms to model the behavior of microcavity polaritons using various approximations.

The early numerical simulations on microcavity polaritons had emphasis on studying the behavior of the low-density system in order to understand the interplay between the relaxation rates and the recombination rates. Tassone *et al.*[18] used a model with only polariton-phonon scattering and polariton decay (which occurs by emission of a photon which leaves the cavity), taking into account the angle-dependent behavior of the Bragg mirrors used to make the microcavity. They concluded that photoluminescence decay times increased with temperature while rise times following a laser excitation pulse decreased. Neither was significantly affected by detunings of up to twice the Rabi splitting (the energy splitting between the upper and lower polariton states). Their calculations indicated that the excitonic region of the lower polariton was nearly thermalized, but that relaxation to the lower energy states may be inhibited, the so-called polariton bottleneck effect,[19] also observed in the dynamics of excitons and polaritons in bulk crystals.[20] Later work,[21] which included a nonresonant pumping term, calculated the formation rate of the lower polaritons as a function of polariton energy, again only taking into account scattering with acoustic and optical phonons.

At high particle density, polariton-polariton scattering rates become important (the scattering rate is proportional to n). This was numerically considered by Tassone and Yamamoto,[22] in addition to phonon scattering. Polaritons interact through their excitonic component.[9] Exciton-exciton scattering rates are not exactly known, but have been estimated by various approximate calculations[9,23–26] to be short range, with s-wave scattering length of the order of the exciton Bohr radius. The main difficulty with calculating the exciton-exciton interaction is the exchange between both electrons and holes. Recent work[27,28] has also shown the importance of exciton-exciton correlation in the effective exciton interaction in a two-dimensional (2D) system.

Tassone's and Yamamoto's publication[22] provides useful insight for those researchers doing a numerical simulation. They describe four criteria important for determining the step size for the energy bins (these conditions were also implicit in Refs. 14, 15, and 17). These are: (1) $\Delta E \ll k_B T$. The distribution functions, which at low density are proportional to $\exp(-E/k_B T)$, are best approximated by small steps of energy. (2) $\Delta E \ll \hbar c \bar{q}$, where $\bar{q}$ is the average phonon momentum exchanged. (3) Results should not vary with changes in ΔE. When ΔE is low enough, the results become independent of the choice of ΔE. (4) $\Delta E > \hbar\Gamma$, where Γ is the rate of change in the polariton distribution. As discussed in Ref. 13, Sec. 4.8, the Boltzmann equation, such as Fermi's golden rule, assumes that the time scale for change in the distribution function is slow compared to $\hbar/\Delta E$, where ΔE is an energy range which may be considered to have constant occupation number.

Malpuech *et al.*[29] explored free electron-polariton scattering in addition to polariton-polariton and polariton-phonon scatterings. The dipole-charge scattering matrix element for electrons interacting with excitons is larger than that for exciton-exciton interaction.[30,31] With this mechanism included, Malpuech *et al.* were able to show large populations in the lower polaritons near $k=0$. A year later a model was published showing coherence in the ground-state buildup.[32]

In a series of papers,[33–36] Doan and co-workers showed the possibility of large accumulations in the polariton ground state. The first paper[33] showed that with the correct choice of parameters it is theoretically possible for acoustic phonons to overcome the bottleneck. They chose cavity lifetimes of 50 ps as opposed to typical lifetimes of current samples of a few picoseconds. In Ref. 36, a similar study was done for II-VI materials. By treating the lowest states as discrete states instead of a continuum, this group was able to show a steady-state Bose-Einstein distribution could occur.

Porras *et al.*[37] followed Tassone and Yamamoto's 1999 model[22] with some simplifications to the numerics. Many models assume that the polaritons are interacting with a phonon bath at constant temperature. The interaction of polaritons with phonons is a quick calculation compared to the time taken to calculate the interaction with lower polaritons and low-energy excitons. One way to speed up the calculation is to separate the lower polariton dispersion curve into a polariton region and a thermalized exciton region. Thus, for the exciton region,

$$n_{xi} = n_x e^{-\beta \epsilon_{xi}} \tag{2}$$

with n_x the occupation number for the lowest energy exciton, $\beta = k_B T$, with T the exciton temperature and ϵ_{xi} the energy of excitons with higher energy. In this model, the populations become disjoint at the bottleneck and this bottleneck region is neglected.

To further simplify the system they used a quantized area. As in the case of Refs. 33–36, this causes the wave vectors to be discrete. They also did the calculation in k space instead of energy space. This makes it easier to have a large number of low energies, the main region of interest. In three dimensions, the equations can be analytically reduced further in energy space than in k space. In two dimensions there is an integral that cannot not be simplified, which makes doing the calculation in k space equivalent to doing the calculation in energy space.

They were able to show that their model reproduces the calculations of Tassone and Yamamoto[22] at low densities. They were also able to show, using parameters consistent with CdTe, that large occupation numbers in the lower polariton states could be achieved with pumping levels as high as 1.5×10^{11} cm^{-2}. This density is 20 times greater than what Tassone and Yamamoto used but is less than Porras's calculated saturation density of 6.7×10^{11} cm^{-2}.[37]

Chaves and Rodriquez[38] included polaritons scattering with free electrons as well as scattering with acoustic phonons but ignored polariton-polariton scattering mechanisms. They, too, were able to show that transition beyond the bottleneck region was possible. They did not provide the details of the polariton-electron scattering matrix element.

Some of the most elaborate models have started with a condensed phase already present and then take into account a Bogoliubov transformation.[39,40] Sarchi and Savona's model follows along a path worked out for atomic condensates discussed in Refs. 41 and 42. In these studies not only do they keep track of occupation numbers but allow the dispersion relationship to shift in the energy due to particle-particle interactions. Their method breaks the population up into three

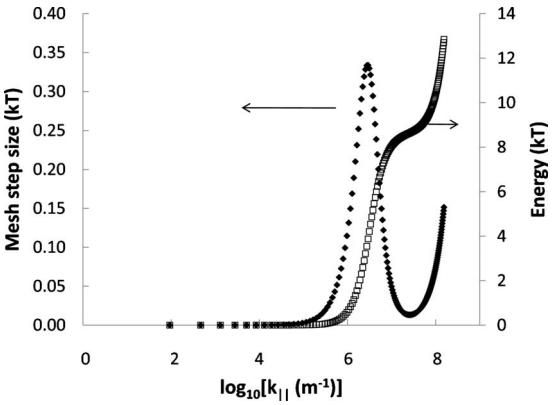

FIG. 1. The energy step size as a function of wave number on the mesh. The dispersion curve for the polaritons is plotted on the secondary vertical axis.

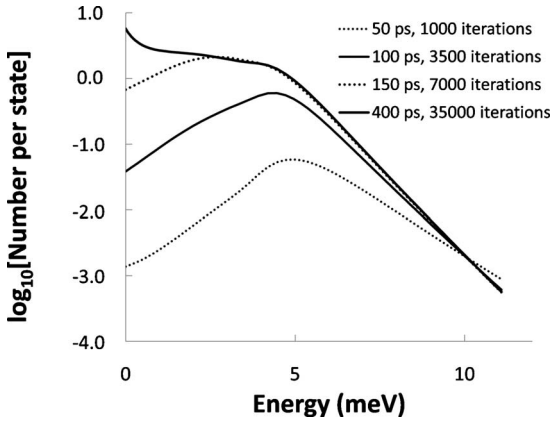

FIG. 2. Evolution of the energy distribution of the exciton polaritons for the same parameters as in Fig. 6, below. The number per state before the first iteration was 10^{-7} for all states. The system evolves to steady state by 400 ps of simulated time.

distinct regions: a condensed polariton region, an excited polariton region, and an uncoupled exciton region. Using GaAs parameters, in-plane quantization lengths of between 10 and 30 μm, and a Rabi splitting of around 7 meV, their main conclusion was that cavities need to be designed with only moderately long polariton lifetimes, $\tau_{pol} \sim 10$ ps, to give the possibility of studying thermalized distributions.

All of the numerical simulations discussed in this section have shown that the $k=0$ state can have orders of magnitude more population than more energetic polaritons below the bottleneck. None of these groups have directly compared numerically simulated distribution functions to experimental data. We are interested in directly comparing our experimental data on the distribution function of the polaritons to our data for nonresonant pumping, which extends all the way up to the polariton bottleneck region.

III. NUMERICAL METHOD

To simulate the dynamics of the polaritons we define a mesh in energy space. The mesh is a group of bins; each bin holds the number of particles within the width of that bin for that energy. The whole energy space spans a region up to a point where the highest energies are many times that of the modeled lattice temperature, typically $E_{max} \sim 10k_BT$. This ensures that the highest energy has a very low occupation number; it acts as a boundary condition to control the simulation. Since the dispersion curve for the polaritons is somewhat flat for low energies, the mesh spacing has very many points near $k=0$, then becomes sparse just below the bottleneck region, and then becomes dense again for the flat exciton region. The number of points is chosen so that the largest ΔE remains well below the thermal energy. A plot of bin width versus wave number is given in Fig. 1.

Once this mesh has been defined, then an average occupation per state at each energy bin is assigned. The laser generation is modeled by direct creation of particles with a time-dependent term $P_{\vec{k}}(t)$. In the present case, since we were simulating the laser being nonresonant, greater than 100 meV above the lower polariton energies, we assumed that the free electrons and holes created in this process enter all the exciton-polariton states in the lowest band with equal probability. Another model[21] shows that when the system is pumped far above the polariton energies that all states, lower polariton and exciton, are populated at a rate within the same order of magnitude. Additionally, we modeled pumping only the excitonic states with a Boltzmann distribution having a temperature ten times greater than the lattice temperature and with the same pump density as in our uniform pumping method. The steady-state solution was the same in both cases, and we concluded that the solution does not depend strongly on the exact energy distribution of the generated particles.

After the initial assignment, the simulation calculates the scattering rate in and scattering rate out for each bin on the mesh. Then the occupation number of each bin is updated. The amount of change is such that the whole system has a certain fraction of particles redistributed. Each bin's change, Δn_k, is proportional to its respective $\partial n_k/\partial t$. The simulation then calculates what time step is needed to move a certain fraction of the total population and updates according to the rule

$$\Delta n_k = \frac{\partial n_k}{\partial t}\Delta t, \tag{3}$$

which is a reasonably good approximation if Δt is small enough. The overall rate of change is described by Eq. (1). This process of calculating the changes to n_k continues in a loop with the new $n_{\vec{k}}$ used to find the new $W_{\vec{k}\to\vec{k}'}(t)$ in each iteration until a steady-state distribution is obtained. Figure 2 gives a typical example of the evolution toward steady state.

Because the quantum Boltzmann equation keeps track of only the average particle number per state and not coherence, we can only apply this method to the range of polaritons densities below the critical threshold for onset of coherence. Nevertheless, we can apply it to data just at the cusp of coherence. The simulations show that the Bose statistics of the particles play a crucial role in the buildup of particles in low-energy states.

TABLE I. Material constants used in the numerical model.

Parameter	Value	Reference
Exciton binding energy, E_B	0.01 eV	43
Longitudinal phonon speed of sound, u	5.117×10^5 cm/s	44
Transverse phonon speed of sound, u	3.012×10^5 cm/s	44
Pikus-Bir coefficient, b	1.8 eV	44
Pikus-Bir coefficient, d	5.4 eV	44
Optical phonon frequency, ω_{LO}	1.07×10^{13} Hz	44
GaAs longitudinal-acoustic-phonon deformation potential, electron, a_e	−7.0 eV	45
GaAs longitudinal-acoustic-phonon deformation potential, hole, a_h	2.7 eV	45
GaAs electron mass, m_e	$0.67m_e$	46
GaAs hole mass, m_h	$0.18m_e$	46
GaAs piezoelectric e_{14}, e_{25}, e_{36}	−0.16 C/m^2	47

Our model includes three types of interactions: polariton-polariton, polariton-phonon, and polariton-electron. The following sections describe how these scattering rates are calculated. The equations presented use various choices of parameter and material constants. Table I provides a list of material constants used in our simulations and Table II provides a list of experimental parameters.

A. Polariton-polariton interactions

The net out-scattering rate of the occupation number $n_{\vec{k}_0}$ of state $\vec{k}_0$ is given by

$$\frac{\partial n_{\vec{k}_0}}{\partial t} = \frac{2\pi}{\hbar}\sum_f |\langle f|V_{int}|i\rangle|^2 \delta(E_f - E_i), \tag{4}$$

where two particles scatter from state $|i\rangle=|\vec{k}_0\vec{k}_3\rangle$ to state $|f\rangle=|\vec{k}_2\vec{k}_1\rangle$. This is done through a scattering interaction V_{int}, which for a two-body elastic-scattering process is

$$V_{int} = |M| a^\dagger_{\vec{k}_1} a^\dagger_{\vec{k}_2} a_{\vec{k}_3} a_{\vec{k}_0}, \tag{5}$$

where M is the matrix element for the interaction and $a^\dagger_{\vec{k}}$ and $a_{\vec{k}}$ are creation and operators for polaritons, which are here considered to be pure bosons (for issues of the composite nature of the bosons, see Refs. 48 and 49). The action of the creation and destruction operators becomes, after operating on a bosonic Fock state,

$$\langle f|V_{int}|i\rangle = |M|\sqrt{n_{\vec{k}_0} n_{\vec{k}_3}(n_{\vec{k}_2}+1)(n_{\vec{k}_1}+1)}. \tag{6}$$

Squaring this term and putting it back into the scattering rate, Eq. (4), gives the scattering out of state $\vec{k}_0$,

$$\frac{\partial n_{\vec{k}_0}}{\partial t} = \frac{2\pi}{\hbar}\sum_{\vec{k}_1\vec{k}_2} |M(|\vec{k}_0 - \vec{k}_2|)|^2 n_{\vec{k}_0} n_{\vec{k}_3}[1+n_{\vec{k}_1}][1+n_{\vec{k}_2}] \times \delta[E(\vec{k}_0)+E(\vec{k}_3)-E(\vec{k}_2)-E(\vec{k}_1)], \tag{7}$$

where $\vec{k}_3$ has been eliminated by momentum conservation, $\vec{k}_3+\vec{k}_0=\vec{k}_1+\vec{k}_2$. The sums over $\vec{k}_1$ and $\vec{k}_2$ can be converted to integrals by taking the thermodynamic limit,

$$\frac{\partial n_{\vec{k}_0}}{\partial t} = \frac{S^2}{(2\pi)^3\hbar}\int d^2\vec{k}_1 d^2\vec{k}_2 |M(|\vec{k}_0 - \vec{k}_2|)|^2 n_{\vec{k}_0} n_{\vec{k}_3}[1+n_{\vec{k}_1}] \times [1+n_{\vec{k}_2}]\delta[E(\vec{k}_0)+E(\vec{k}_3)-E(\vec{k}_2)-E(\vec{k}_1)], \tag{8}$$

where S is the area of the sample. We assume the system is

TABLE II. Numerical model parameters.

Parameter	Value	Comments
Exciton Bohr radius, a_B	130 Å	Calculated from exciton binding energy, $a_B = e^2/4\pi E_B\epsilon$
Quantum-well width, L_z	7 nm	Growth parameter for samples used in Ref. 3
Number of bins in mesh	170	Needed for numerical accuracy
Width of lowest energy bin	$4.79\times10^{-12}k_BT$	Needed for numerical accuracy
Rabi splitting, Ω_R	14.95 meV	Experimentally measured
Cavity lifetime	5 ps	Concluded from analysis
Exciton lifetime	>400 ps	Steady state not affected by lifetimes longer than this

isotropic in k space. Then $n_{\vec{k}}=f[E(\vec{k})]$, which is independent of the difference in directions of the $\vec{k}$'s (θ, as described in Appendix A), and $n(E)=n_{|k|}=f[E(\vec{k})]D[E(\vec{k})]dE$, where $D(E)dE$ is the number of states within dE of E. The density of states $D(E)=Sgm/(2\pi\hbar^2)$, where g is the state degeneracy (equal to 2 here) and m is the effective mass of the polariton for E. The change to the number of particles within dE of E_0 per unit time for scattering out of a state is

$$\frac{\partial n(E_0)}{\partial t}=\frac{S^2D(E_0)}{(2\pi)^3\hbar}dE_0\int d^2\vec{k}_1d^2\vec{k}_2|M(|\vec{k}_0-\vec{k}_2|)|^2f(E_0)f(E_3)\times[1+f(E_1)][1+f(E_2)]\delta(E_0+E_3-E_2-E_1). \quad (9)$$

This equation can be analytically simplified to reduce the numerical work necessary to solve it. As shown in Appendix A, it can be reduced to an integral over two energies and one angle. A similar integral is obtained for the in-scattering rate. The difference is in the statistical factors, which become

$$f(E_1)f(E_2)[1+f(E_0)][1+f(E_3)].$$

The integral for $\partial n(E)/\partial t$ can then be evaluated numerically. The integral over θ_2 can be done with Gaussian quadrature, which speeds up the calculation. Additionally, the transformation for Gaussian quadrature avoids the poles that result from integrating over θ_2. The table for calculating the abscissa points and weights for the Gaussian quadrature were taken from Ref. 50. This book also gives a good review of the theory behind Gaussian quadrature.

The polariton-polariton interaction matrix element, $M(|k_0-\vec{k}_2|)$, was studied by Ciuti *et al.*[51] Only the excitonic components of the polaritons are interacting. A factor $X_{k,k'}$ is used in the interaction model to account for this, which stands for the product of the X_k Hopfield coefficients for the participating polaritons (see Ref. 9). There are four polaritons involved here, so $X_{k,k'}=X_{\vec{k}_0}X_{\vec{k}_1}X_{\vec{k}_2}X_{\vec{k}_3}$. Using $\phi_{\vec{k}}$ for the 2D excitonic wave function, the matrix element M is then given by

$$M=\frac{1}{S}\sum_{\vec{k}\vec{k}'}X_{k,k'}V_{\vec{k}-\vec{k}'}\phi_{\vec{k}}\phi_{\vec{k}'}(\phi_{\vec{k}}^2-\phi_{\vec{k}}\phi_{\vec{k}'}). \quad (10)$$

The interaction potential, $V_{\vec{k}-\vec{k}'}$, is proportional to $1/|\vec{k}-\vec{k}'|$ for two-dimensional Coulomb interactions and $\phi_{\vec{k}}=\sqrt{8\pi a_B^2/S}(1+k^2a_B^2)^{-3/2}$. An approximation for M, accounting for exchange, was determined by Tassone and Yamamoto[22] to be

$$M\sim 6X_{k,k'}E_B\frac{a_B^2}{S}. \quad (11)$$

This approximation was used in our models.

B. Polariton-phonon interactions

1. Longitudinal-acoustic phonons

The scattering process discussed in the last section was a four-body process in two dimensions. The process discussed in this section is a three-body process in which the polaritons are constrained to two dimensions but the phonons are three dimensional. The polariton-phonon model is based on the exciton-phonon interaction,[46] which itself is based on the standard electron-deformation potential interaction.[13] The hydrostatic deformation potential interaction in this case has the form

$$M(\vec{k},\vec{q})=iX_{k,k'}\sqrt{\frac{\hbar(q_\parallel^2+q_z^2)^{1/2}}{2\rho Vu}}\times[a_eI_e^\parallel((|\vec{q}|)I_e^\perp(q_z)-a_hI_h^\parallel(|\vec{q}|)I_h^\perp(q_z)], \quad (12)$$

where ρ, V, u, and q are the material density, volume, longitudinal sound velocity, and phonon wave number, respectively, and the I's are overlap integrals, defined below. The hydrostatic deformation potentials for each band are a_e and a_h, and are taken to be the bulk value for GaAs, $a_e=-7$ eV and $a_h=2.7$ eV.[45] The $X_{k,k'}$ is the product of two Hopfield coefficients here since there are only two polariton states involved (the initial and final state).

The overlap integrals between the excitons in the quantum wells and the phonons in the bulk are found, using the envelope function approximation[21,43,46,52,53] to be

$$I_{e(h)}^\perp(q_z)=\frac{8\pi^2}{L_zq_z(4\pi^2-L_z^2q_z^2)}\sin\left(\frac{L_zq_z}{2}\right) \quad (13)$$

and

$$I_{e(h)}^\parallel=\left[1+\left(\frac{m_{h(e)}}{2M}|q_\parallel|a_B\right)^2\right]^{-3/2}, \quad (14)$$

where L_z is the quantum-well thickness.

The out-scattering process for state $\vec{k}$ while creating a phonon is given by

$$\frac{\partial n_{\vec{k}}}{\partial t}=\frac{2\pi}{\hbar}\sum_{\vec{k}_1,\vec{q}_z}|M(\vec{k},\vec{q})|^2n_{\vec{k}}[1+n_{\vec{k}_1}][1+n_{\vec{q}}]\times\delta[E(\vec{k})-E(\vec{q})-E(\vec{k}_1)]. \quad (15)$$

The in-plane momentum has been conserved through $\vec{q}_\parallel=\vec{k}-\vec{k}_1$ with $\vec{q}=\sqrt{\vec{q}_z^2+\vec{q}_\parallel}$. As with the polariton-polariton scattering, this integral can be reduced substantially analytically, as shown in Appendix B.

There are three other possibilities for phonon interaction. These are scattering out of a state $\vec{k}$ while absorbing a phonon, scattering into a state $\vec{k}$ while emitting a phonon, and scattering into a state $\vec{k}$ while absorbing a phonon. Two of these processes are the inverse of the other two and that symmetry is used as a check on the numerical calculation.

2. Transverse-acoustic phonons

The polaritons interact with transverse-acoustic phonons as well. Essentially the scattering is the same as for scattering with longitudinal phonons but transverse phonon values are used. We do not account for polarization; Ref. 15 showed that the effective deformation potential, Ξ, for transverse phonons can be given by

$$\Xi = \left[\frac{4}{5}\left(b^2 + \frac{d^2}{2}\right)\right]^{1/2} \tag{16}$$

with b and d as deformation potentials in the Pikus-Bir notation.[54] Measurements on GaAs show the holes to have $b=1.8$ eV and $d=5.4$ eV.[44] The electrons have $b=0$ and $d=0$ since the conduction band is s like. Since there are two directions of polarization for transverse phonons, a factor of 2 is included in the polariton-transverse phonon-scattering calculation.

3. Piezoelectric phonon interactions

The matrix element for polaritons interacting with phonons through piezoelectricity is given by

$$M(|\vec{k},\vec{q}|) = X_{k,k'}\frac{e}{4\pi\epsilon}\sum_{\lambda}\sum_{ijl} e_{ijl}\frac{q_i q_j}{q^2}\eta_{(q\lambda)l}\sqrt{\frac{\hbar}{2\rho V\omega_{q\lambda}}} \times [I_e^{\parallel}(|\vec{q}|)I_e^{\perp}(q_z) - I_h^{\parallel}(|\vec{q}|)I_h^{\perp}(q_z)], \tag{17}$$

where ρ, V, and q are the material density, volume, and phonon momentum, respectively, η is a unit vector for the polarization of a phonon with momentum $\vec{q}$ and polarization index λ, e_{ijl} is the piezoelectric tensor for the material being considered and the I's have been defined in Eqs. (13) and (14). Here we have adapted the standard piezoelectric interaction[13] to the case of quantum wells, as for the cases above.

When two or more terms describe interactions of the same particle types, e.g., acoustic phonons with polaritons in this section and the previous sections, the terms must be added before squaring and using them in the quantum Boltzmann equation. However, the deformation potential is an imaginary term while the piezoelectric term is real. Thus, they are completely out of phase with each other and there are no mixed terms upon squaring.

Squaring the above M gives, using u, the speed of sound, and $\omega=\hbar u q$,

$$|M|^2 = \frac{X_{k,k'}^2}{32\pi^2\rho V u}\sum_{\lambda}\sum_{ijl} e_{ijl}^2\frac{\eta_{(q\lambda)l}^2 e^2}{\epsilon^2}\frac{q_i^2 q_j^2}{q^5} \times [I_e^{\parallel}(|\vec{q}|)I_e^{\perp}(q_z) - I_h^{\parallel}(|\vec{q}|)I_h^{\perp}(q_z)]^2. \tag{18}$$

For GaAs, e_{ijl} only has three nonzero values: $e_{14}=e_{25}=e_{36}=-0.16$ C/m^2 (Ref. 47) (in reduced notation[13]). Since all three indices must be different, the polaritons only have piezoelectric interaction with transverse phonons. Performing the sum over i, j, and l gives

$$M^2 \propto \frac{2}{q^5}(q_x^2 q_y^2 + q_x^2 q_z^2 + q_y^2 q_z^2). \tag{19}$$

In cylindrical coordinates this becomes

$$M^2 \propto \frac{2}{q^5}(q_z^2 q_{\parallel}^2 + q_{\parallel}^4 \cos^2\theta_q \sin^2\theta_q). \tag{20}$$

The angle θ_q is measured with respect to the polariton wave vector $\vec{k}$ in the $q_{\parallel}$ plane. To simplify the numerical calculation we find the average magnitude of the trigonometric terms, which is

$$\langle \cos^2\theta_q \sin^2\theta_q \rangle = \frac{1}{2\pi}\int d\theta_q \cos^2\theta_q \sin^2\theta_q = \frac{1}{8}. \tag{21}$$

The total matrix element squared for piezoelectric scattering is then

$$|M|_{piezo}^2 = \frac{X_{k,k'}^2}{16\pi^2\rho V u}\frac{e_{14}^2 e^2}{\epsilon^2}\frac{q_{\parallel}^2\left(q_z^2 + \frac{q_{\parallel}^2}{8}\right)}{q^5} \times [I_e^{\parallel}(|\vec{q}|)I_e^{\perp}(q_z) - I_h^{\parallel}(|\vec{q}|)I_h^{\perp}(q_z)]^2. \tag{22}$$

The piezoelectric phonon interaction is inversely related to the momentum exchanged. Our estimates conclude that the piezoelectric interaction is stronger than the deformation-potential interaction for small exchanges. When considering all possible interactions, however, by using the simulation, we found the piezoelectric scattering to be only a small term. The model results were essentially the same with or without the piezoelectric interaction as parameters were varied. This is because most of the piezoelectric interaction happens within the k space defined by the width of each bin. Nevertheless, we kept the scattering mechanism in the total model. This is primarily because the phonon scattering is easily calculated and including the piezoelectric effect only increased the time required to process the simulation by 2%.

4. Optical phonons

The simulations here did not use a Frohlich interaction; the polaritons are at low temperature. Optical phonons in GaAs have $\hbar\omega \cong 36$ meV, which is much greater than $k_B T$. Our code is capable of modeling such an interaction, though. The analytical manipulation of the scattering equation is very similar to the previous sections. The matrix element is given by

$$M(|\vec{k},\vec{q}|) = iX_{k,k'}\sqrt{\frac{2\pi e^2\hbar\omega_{LO}}{(\vec{q}_{\parallel}^2 + q_z^2)V}\left(\frac{1}{\epsilon_{\infty}} - \frac{1}{\epsilon_0}\right)}^{1/2} \times [a_e I_e^{\parallel}(|\vec{q}|)I_e^{\perp}(q_z) - a_h I_h^{\parallel}(|\vec{q}|)I_h^{\perp}(q_z)] \tag{23}$$

with

$$I_{e(h)}^{\perp}(q) = \frac{8\pi^2}{L_z q(4\pi^2 - L_z^2 q^2)}\sin\left(\frac{L_z q}{2}\right) \tag{24}$$

and

$$I_{e(h)}^{\parallel} = \left[1 + \left(\frac{m_{h(e)}}{2M}|q_{\parallel}|a_B\right)^2\right]^{-3/2}. \tag{25}$$

An optical phonon has an almost flat dispersion relationship so we take the optical phonon energy as a constant, $E(\vec{q})=\hbar\omega_{LO}$. The integration with the delta function is the same as for acoustic phonons, in Eqs. (B3)–(B9); the final result for out scattering due to phonon emission is

$$\frac{\partial n_{\vec{k}}}{\partial t} = \frac{e^2 u}{2\pi\omega_{LO}}\left(\frac{1}{\epsilon_\infty} - \frac{1}{\epsilon_0}\right)\int \frac{dE_1 d\theta_1}{\frac{\partial E_1}{\partial(k_1^2)}} X_{k,k'} \times [a_e I_e^{\parallel}(|\vec{q}|) I_e^{\perp}(a) - a_h I_h^{\parallel}(|\vec{q}|) I_h^{\perp}(a)]^2 \times n_{\vec{k}}[1 + n_{\vec{k}_1}][1 + n_{\vec{q}}]. \quad (26)$$

Here, $E - E_1$ has been replaced with $\hbar\omega_{LO}$ and

$$a = \sqrt{\left(\frac{\omega_{LO}}{u}\right)^2 - q_{\parallel}^2} \quad (27)$$

with $\omega_{LO} = 1.07 \times 10^{13}$ Hz for GaAs.[44]

C. Electron-polariton interactions

The matrix elements for direct and exchange interactions for free electron-polariton scattering have been calculated in Ref. 55. This paper shows that the direct term for electron-exciton scattering is much smaller than the exchange term for $\Delta k < 1/a_B$ and $m_e = m_h$. This is reasonable since it can be expected for the free electron to interact equally with the electron and the hole of the exciton. Using the exchange term provided by Ref. 55 was difficult to implement in our numerical model because it depends on several angles between the particle momenta. This, coupled with a desire to use a function that more formally used a screening parameter, prompted us to derive our own approximate form of the interaction.

We start with the 2D excitonic wave function using the symbol k to mean $k_{\parallel}$,

$$\phi(k) = \sqrt{\frac{2a_B^2}{\pi}}\frac{1}{[1 + (ka_B)^2]^{3/2}}. \quad (28)$$

The Hamiltonian term for electron-electron exchange interaction is given by[13,17]

$$H_{ex} = \frac{1}{2S}\frac{e^2}{\epsilon(|\Delta k| + \kappa)} b^{\dagger}_{k-\Delta k} b^{\dagger}_{k'+\Delta k} b_k b_{k'}. \quad (29)$$

Here, κ is the screening parameter and the $b_k^{\dagger}$ and b_k are the creation and destruction operators for electrons, respectively. The Debye-Huckel screening parameter is given by

$$\kappa = -\frac{e^2}{2\epsilon_\infty}\sum_{\vec{k}} \frac{\partial f[E(\vec{k})]}{\partial E}. \quad (30)$$

Substituting a Fermi-Dirac thermalized distribution for $f(E)$ and performing the sum by converting it to an integral results in the two-dimensional Debye screening formula,

$$\kappa = \frac{e^2}{2\epsilon_\infty}\frac{n}{k_B T}, \quad (31)$$

where n is the two-dimensional density of electrons, k_B is Boltzmann's constant, and T is the electron temperature.

Using the exciton wave function for the probability amplitude of each electron state, the matrix element, $M = \langle f|H_{ex}|i\rangle$, becomes the integral,

$$M = \frac{e^2}{\epsilon}\frac{a_B^2}{(2\pi)^2}\int d^2k_e \frac{1}{[(k_2^2 + k_e^2 + \Delta k_2^2 - 2k_2\cdot k_e + 2k_2\cdot\Delta k_2 - 2k_e\cdot\Delta k_2)^{1/2} + \kappa]} \frac{1}{(1 + (k_e^2 + \Delta k_2^2 + 2k_2\cdot\Delta k_2)^2 a_B^2)^{3/2}} \frac{1}{(1 + k_e^2 a_B^2)^{3/2}}. \quad (32)$$

We simplify this by assuming the dot products average to zero. Also, we assume the integration replaces k_e with $1/a_B$ and provides a multiplier of $2/a_B^2$ as determined by numerical integration. The result is

$$M = \frac{\sqrt{2}Se^2}{4\pi^3\epsilon}\frac{1}{[(k_2^2 + (1/a_B^2) + \Delta k_2^2)^{1/2} + \kappa]}\frac{1}{(2 + \Delta k^2 a_B^2)^{3/2}}. \quad (33)$$

As in the other processes, the polaritons interact with the electrons only through their exciton components, so a factor $X_{k,k'}$ must be used for the initial and final polariton states.

This element is placed into the quantum Boltzmann equation as was done in the previous sections. A bath of fermions is assumed to exist which remains a Fermi-Dirac distribution at all times. If high electron density is considered, the statistical terms must take into account the Fermi statistics, namely a $(1-n)$ factor must be used for fermions where a $(1+n)$ factor would be used for bosons.

D. Energy renormalization

The dispersion curve shown in Fig. 1 is the dispersion that a single exciton polariton in the system would have. Once another particle is introduced into the system, there is an interaction between the particles. If the density of particles is high enough, there can be a noticeable change in the dispersion curve.

Our code can take into account the energy shifts discussed below and calculate a new dispersion relationship. The scattering rates depend on the density of states of the particles, which in turn, depend on the dispersion relationship. Without these shifts, all but the statistical parts of the integrals can be done once and saved for all later time iterations. When these energy shifts are taken into account, all parts of the scattering

rate must be recalculated for each time step and the whole calculation proceeds much slower.

There are two basic effects that lead to energy shifts of the polaritons. One is the overall repulsive exciton-exciton interaction, which can be called a mean-field blueshift, although, as discussed above, correlation effects of higher order than the mean-field term have been shown to have important effects on this shift in at least some cases.[27,28] This effect is seen near the critical threshold for condensation of polaritons.[11] A second effect is phase space filling. As the density of particles increases, the states in the sample begin to fill up. Because the excitons are made of underlying fermionic constituents, there is an upper bound to the total number of new exciton polaritons that can be created. As this limit is approached, the excitons start to decouple from the photons. Experimentally, this is seen as the polariton splitting becoming weaker. This leads to a blueshift of the lower polariton line and a redshift of the upper polariton line, i.e., a closing of the line splitting.[4,11]

The results shown here do not use these energy corrections, and therefore the polariton dispersion curve is not renormalized. An overall shift of the polariton energy will not affect the scattering dynamics; only a change in the effective mass due to a k-dependent shift will affect the dynamics. We find experimentally that the change in the effective mass is small in the density range below the critical threshold for condensation.

IV. FITS TO THE EXPERIMENTAL DATA

The parameter space is rather large and includes a number of variables. Nevertheless, we can constrain these parameters with experimental input for a wide variety of conditions; in particular, variation in the pump density.

One relatively unknown parameter is the intrinsic polariton radiative lifetime, which is related to the cavity photon lifetime and the exciton lifetime; the exciton lifetime is so much longer than the photon lifetime in the cavity that we can approximate that the radiative decay rate in the polariton states is entirely dominated by the photon loss rate, and therefore is proportional to the photon fraction of the polaritons (which is 50% at the resonance point and falls as the polaritons become more excitonlike at high momenta.)

It is difficult to extract this number directly from experiments because the rate of decay of the polariton population depends on the net rate of scattering into the polariton region. Therefore we estimate the intrinsic lifetime from the best fits of our simulations to the data. It was found that lifetimes for the cavity mode between 2 and 5 ps gave a steady-state result that most resembled the data. A cavity mode lifetime of 5 ps was used as a fixed value in all these simulations, which is equivalent to a polariton lifetime at resonance of 10 ps, and a population lifetime, for all polariton states up to 3.5 meV above the lowest polariton state, of 14 ps.

The values of the deformation potentials for the transverse- and longitudinal-acoustic phonons are given in the literature for GaAs but they have some uncertainty. The possibility of varying them was investigated but they were kept at the values listed in Table I for the results reported here.

The lattice temperature, the free-electron temperature, the effective polariton-polariton scattering cross section, the effective polariton-electron scattering cross section, and the polariton density and free-electron density are other parameters that can be varied in the simulation. The lattice temperature was not strictly known. The helium bath temperature gives a lower bound but in experiments with laser excitation of semiconductors it is quite common for a local region to have temperature well above the bath temperature. In our simulations, our best fits implied lattice temperatures from 4 up to 30 K.

One remaining parameter was a single overall scaling factor. The simulation gives occupation numbers in absolute values. The experimental data for the occupation numbers comes from taking the light emission spectrum as a function of external observation angle; the external angle of an emitted photon corresponds to a single in-plane momentum of the polariton which emitted that photon. The light intensity is divided by the angle-dependent emission rate[9] to get a number proportional to the polariton occupation number. A scaling parameter is used to shift the experimental data for the polariton occupation number, which is in arbitrary units, to the simulation's results. This scaling factor must be the same for all the different sets of data for different laser powers since it depends only on the intrinsic photon-emission matrix element and the geometric collection efficiency factors.

Methods of searching the parameter space were explored, for example, the implementation of the Nelder-Mead method was tried. These methods often resulted in good fits to either the high-density data or to the low-density data but not both simultaneously. The fits were thus made by searching the parameter space through trial and error. Experience and careful analysis of the numerical simulation's results led to finding the best parameters for lattice temperature, polariton-polariton scattering cross section, and the overall data scaling value; in the case of electron scattering with polaritons there were was one additional parameter, the combined value of polariton-electron cross section and the free-electron density. On one hand there is a large parameter space, but on the other hand, we have a large amount of data at many densities which must be fit, so the parameters were tightly constrained.

A. Fits with polariton-polariton and polariton-phonon scatterings only

The initial best fits were done using only polariton-polariton and polariton-phonon scatterings. It was found by increasing the polariton-polariton scattering rate and adjusting the lattice temperature that these two scattering mechanisms were sufficient. Figures 3 and 4 show the results of these fits.

Two experimental pumping conditions were modeled. Under continuous wave (cw) pumping, the fit lattice temperature had to be increased with increasing pump power. This is to be expected since pumping in cw mode was observed to give noticeable shifts of temperature. To avoid this temperature rise during the experiments, the pump laser was chopped

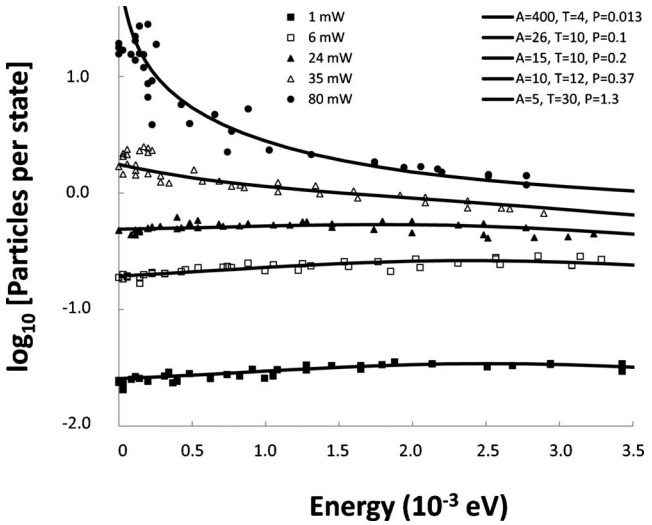

FIG. 3. A fit to the cw pumped data using polariton-polariton and polariton-phonon scatterings. "A" stands for the coefficient used in front of the polariton-polariton scattering cross section and "P" is the generation rate used. Simulated plots are shown next to their corresponding experimental pump power.

with an acousto-optic cell to give a 2.5% duty cycle, but with the pump on for times very long (typically hundreds of nanoseconds) compared to the polariton lifetime (5–10 ps). This quasi-cw data could be fit with the lattice temperature set at 4 K for all generation rates.

As seen in these figures, all the data could be fit by varying the polariton-polariton scattering cross section. A plot of the magnitude of the scattering rate used for the polariton-polariton interaction versus polariton density is shown in Fig. 5. At low density for cw and for quasi-cw the necessary coefficient to the scattering rate is inversely proportional to

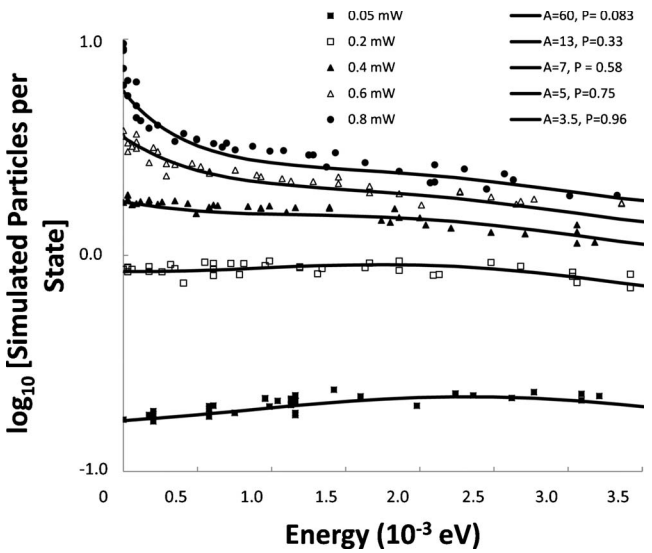

FIG. 4. A fit to the quasi-cw pumped data using polariton-polariton and polariton-phonon scatterings. A stands for the coefficient used in front of the polariton-polariton scattering cross section and P is the generation rate used. Simulated plots are shown next to their corresponding experimental pump power.

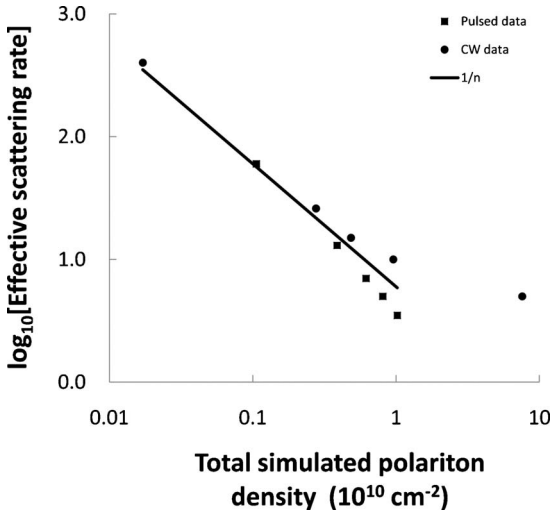

FIG. 5. Plot of the coefficient used for the polariton-polariton scattering matrix element as a function of simulated polariton density.

the density of the polaritons. This is likely unphysical, however, because the polariton-polariton scattering cross section should be a constant, independent of the density. The need for the increasing cross section as density drops comes from the fact that the polariton steady-state distribution stays nearly the same as density approaches zero, as seen in Figs. 3 and 4. One might expect that as the polariton-polariton scattering becomes unimportant at low density, only polariton-phonon scattering is important. Our simulations show, however, that polariton-phonon scattering alone is completely inadequate to give the observed energy distributions, as seen in Fig. 6.

Figure 6 shows several important things about the polariton system in general. First, the three regions of the energy distribution have very different properties. At high energy, which corresponds to the excitonic range of the spectrum, there is a thermalized tail which fits a Maxwell-Boltzmann

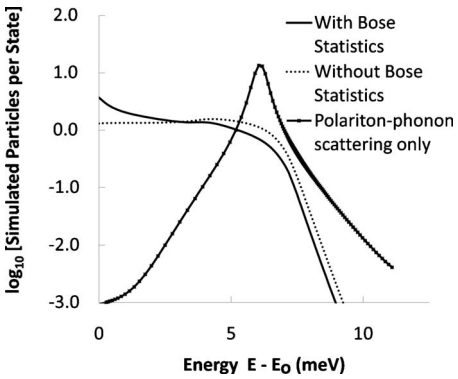

FIG. 6. Solid line with symbols: the low-density steady-state distribution of polaritons in a typical case, when only the polariton-phonon interaction is considered. Dashed line: the same simulation when polariton-polariton interactions are included but the Bose final states $(1+n_k)$ are artificially (unphysically) turned off in the simulation. Solid line: the same simulation when the Bose final states factors are turned on.

distribution [$\exp(-E/k_BT)$ fits a straight line on a semilog plot]. The temperature of this distribution is very close to the lattice temperature. At low energy, which corresponds to the polaritonic region, the polaritons have a nearly thermal distribution with a temperature well above the lattice temperature. As seen in Fig. 6, the Bose statistics of the particles plays an important role in causing this region to fill up with particles and showing the upturn in the occupation number which is characteristic of a Bose-Einstein distribution—when the Bose-Einstein statistical factors are artificially turned off in the computer code, the energy distribution in low-energy states is flat, with no upturn or peak at low energy. Connecting the excitonic and polaritonic regions is the "bottleneck" region. Particles continually stream down from the excitonic region into the polaritonic region through this bottleneck. Because of this, there is no possibility of having the entire distribution have a single temperature, and so the polariton energy distribution will always have a hot tail to high energy, even when it is well thermalized at lower energies.

Another group has also reported[56] the result that the energy distribution remains nearly the same as the density decreases. In Ref. 56, this was modeled as due to inhomogeneous broadening of the energy of the particles. We have run our simulation, replacing the energy delta function in Eq. (4) with a Lorentzian, i.e.,

$$\delta(E) \to \frac{\Delta E}{E^2 + \Delta E^2} \tag{34}$$

but we have not been able to reproduce the experimental results with this method. More generally, replacing the delta function with a Lorentzian is problematic since it leads to violation of energy conservation in the limit of infinite particle lifetime. This can easily be seen in the following argument: suppose that the gas of particles is at $T=0$ in the ground state. In the next time step, some particles will scatter up to higher energy, but none can scatter lower, since they are already in the ground state. Thus the average energy of the gas will increase. Over time, if there is no removal of particles, the energy will always increase.

An *ad hoc* Lorentzian energy broadening may be a useful approximation for the case of finite-lifetime particles with strong disorder. However, in our samples with low disorder (<1 meV) it is unlikely that this can explain our energy distributions at low density. We therefore turned to see if a small population of free electrons can explain the results.

Elastic scattering from disorder will not lead to energy broadening of the polariton distribution, because this type of scattering only randomizes the polariton momentum, while conserving the energy of the polaritons. This process would just contribute to making the polariton distribution more isotropic in k space, but we already assume the distribution is isotopic in k space in this simulation.

B. Fits including electron-polariton scattering

Experimental studies[19,57] have shown that electron-polariton scattering can lead to efficient thermalization of polaritons. When polariton-electron scattering was included, we found we could get good fits at high density with a constant polariton-polariton cross section, with a value about 20% greater than the literature value [see Eq. (11)]. We then found the cross-sectional coefficient for the electron-polariton interaction that would match the lower-density polariton data with a nearly constant density of electrons, which we estimated to be around $\sim 2\times 10^8$ cm^{-2}.

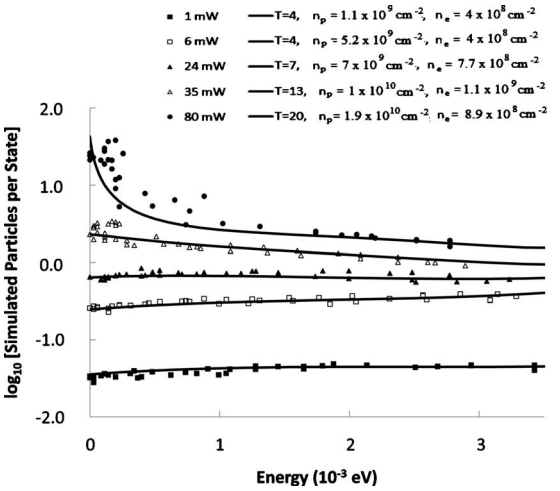

FIG. 7. The final fits to the cw experimental data. In the legend, T stands for the simulated lattice temperature, n_p is the simulated polariton density, and n_e is the simulated electron density. Simulated plots are shown next to their corresponding experimental pump power.

Using a constant value for the polariton-polariton cross section, we found that we could fit all the data if we allowed the lattice temperature and free-electron density to vary over reasonable ranges. Figures 7 and 8 show the results of these fits. The same polariton-polariton scattering cross section was used for both the cw and quasi-cw fits. As in the fits discussed in the previous section which did not include the

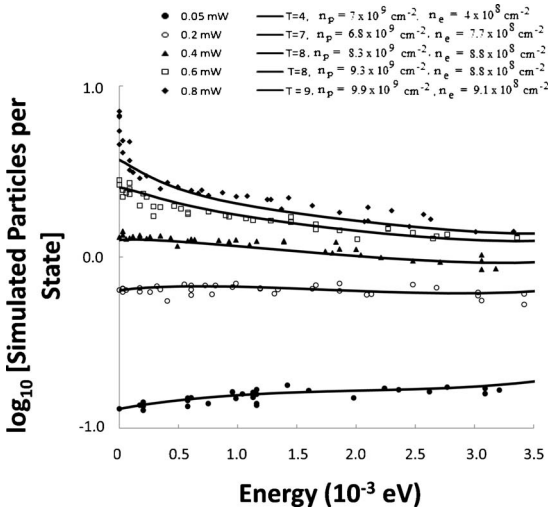

FIG. 8. The final fits to the quasi-cw experimental data. In the legend, "T" stands for the simulated lattice temperature, "n_p" is the simulated polariton density, "n_e" is the simulated electron density. Simulated plots are shown next to their corresponding experimental pump power.

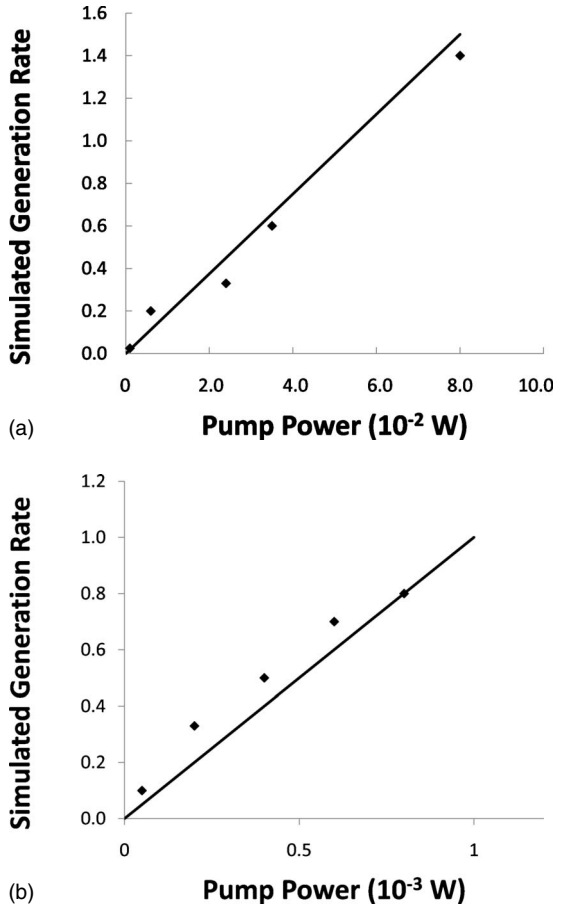

FIG. 9. (a) Plot of the simulated generation rates versus the corresponding experimental pump powers for the cw excitation case of Fig. 7. The line is a guide for the eye. (b) The same rates for the quasi-cw case of Fig. 8. The line is a guide for the eye.

polariton-electron interaction, the fits to the cw data again have a larger lattice temperature increase at higher pump power than the fits for the quasi-cw data. One check on the validity of these fits is that the generation rate determined by the fits is proportional to the experimental pump laser power. Figure 9 shows how the chosen simulated generation rates correlate to the experimental pump intensity for these two sets of data. Essentially, the fits show a linear dependence.

These fits imply an absolute value for the polariton density, not just a relative occupation number, because the Bose effects which lead to the peaking at the low-energy states only occur near the Bose condensation phase boundary. The fitted steady-state polariton densities as a function of the generation rate are shown in Figs. 10 and 11 for the same fits as shown in Figs. 7 and 8. The polariton density begins to saturate with increasing pump power. This is to be expected. As the density increases, the polaritons begin to occupy lower momentum states due to the Bose statistics. These states have shorter lifetimes than the higher energy states and the result is that the average lifetime decreases.

As seen in Fig. 11, the electron density implied by the fits is nearly constant as the pump power is varied, as expected since the photogeneration process creates only neutral electron-hole pairs and no excess charge. The fit value used

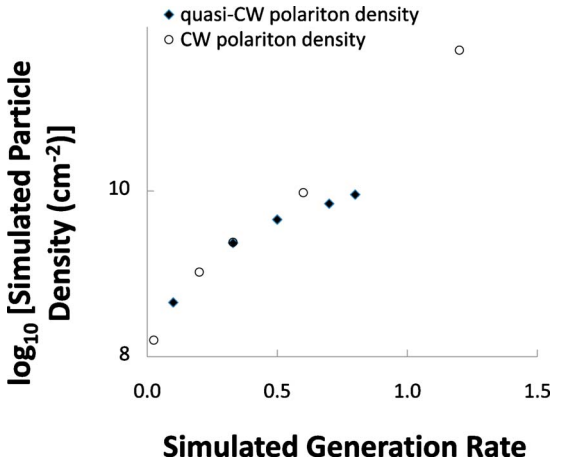

FIG. 10. (Color online) Plot of the steady-state simulated polariton density as a function of simulated generated rate for the data fits of Figs. 7 and 8.

here is approximately 7×10^{8} cm^{-2}. The fit value of the electron-polariton scattering cross section was a constant factor of 30 times larger than the value for the theory presented above [Eq. (33)]. There is a large amount of uncertainty in the cross section for electron-polariton scattering.[17] Since both the electron density and the cross section for electron-polariton scattering are unknown, we cannot use either of these to constrain a value for the other.

In unstressed samples, the amount of thermalization of the polaritons into low-energy states is found experimentally to be much lower at low excitation density, even when at the resonant point when the polaritons should interact strongly with each other through their exciton components. This leads us to believe that the stress induces a population of free carriers. One possible source of a stress-induced electron density is due to effect of stress on the interface between the GaAs and GaAlAs making the quantum wells.[58] The stress used in the experiments can create a piezoelectric polarization in each material. At the interface there is a polarization mismatch. This mismatch can manifest itself as a surface charge. The amount of charge can be estimated by the following method.

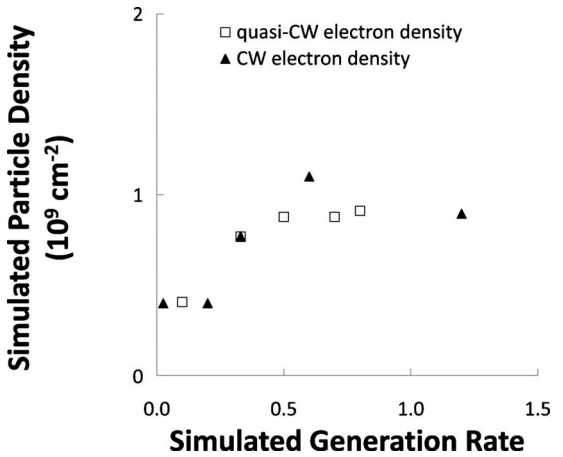

FIG. 11. Plot of the total simulated free-electron density as a function of simulated generated rate.

As discussed elsewhere,[59] the strain in the sample can be accurately calculated by using the Pikus-Bir deformation potentials for GaAs and the measured stress-induced shift of the polariton bands. For a stress-induced polariton band shift of about 15 meV, as in our experiments, then the strain is on the order 10^{-4}. The polarization field, P, induced by piezoelectricity in a material is given by

$$P_i = e_{ij}\epsilon_j, \tag{35}$$

where e_{ij} is the piezoelectric constant. For $Ga_{0.8}Al_{0.2}As$, $e_{41}=0.173$ C/m^2,[60] and for GaAs, $e_{41}=0.16$ C/m^2.[47] The difference in the two polarizations provides the surface charge at their interface. The estimate is an electron density of 8×10^8 e/cm^2, close to the average value of electron density used in the simulations. Again, though, there is much uncertainty. We have 12 quantum wells in the sample and there are two GaAs-GaAlAs interfaces for each quantum well. This is a possible explanation why the scattering cross section needs to be much larger than the expected value.

Another possibility is that there is a low density of donor impurities. These may contribute electrons if they become ionized by local electric fields caused by the stress.

V. CONCLUSIONS

The simulations show that we can treat the exciton-polariton band as having three regimes: a thermalized exciton bath at the lattice temperature, a bottleneck region with streaming particles far from equilibrium, and the polariton region near $k=0$ with an effective temperature above the lattice temperature. When the density of the polaritons approaches the critical density, particles pile up in low-momentum states in a way entirely consistent with our model which assumes that polariton-polariton interaction with Bose-Einstein statistics drives the particles into these low-momentum states. Recent theoretical works have shown that lack of complete thermalization does not prevent the polaritons from making a phase transition,[61–63] and this is consistent with the experimental observation of coherence and a bimodal distribution above the critical density.

At low polariton density, the shape of the polariton energy distribution becomes nearly constant, independent of density. This is surprising, because polariton-polariton interactions should become negligible at low density, and polariton-phonon interactions are completely insufficient to create a substantial population of polaritons in low-energy states, because of the polariton bottleneck between exciton and polariton states. The efficient scattering of the polaritons at these low densities can be explained as arising from polariton interactions with a constant density of free electrons (or holes) in the system, which can arise from stress-induced processes or background impurities.

Although there are many parameters in this model, the need to fit a broad range of densities with a single theory, with the same parameters for phonon scattering, polariton-polariton scattering cross section, and intrinsic lifetime strongly constrains the fits. The physical reasonableness of the parameters used here, as well as the success of the fits to the data, indicates that the polaritons are indeed acting as a gas of weakly interacting bosons.

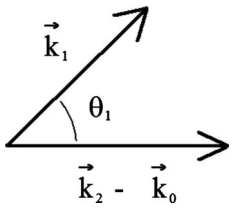

FIG. 12. The angle θ_1 that $\vec{k}_1$ makes to the direction of the difference between $\vec{k}_0$ and $\vec{k}_2$.

ACKNOWLEDGMENTS

This work has been supported by the National Science Foundation under Grant No. DMR-0706331. We thank R. Balili and B. Nelsen for contributions to the experimental data discussed here.

APPENDIX A: TWO-BODY, TWO-DIMENSIONAL ANGLE INTEGRALS

In Eq. (9) we need to integrate over $\vec{k}_1$ and $\vec{k}_2$, or over the variables, $k_1=|\vec{k}_1|$, θ_1, $k_2=|\vec{k}_2|$, and θ_2. The delta-function arguments, E_1, E_2, and E_3 depend on these variables. We pick one variable, θ_1, to integrate out the delta function. We could pick any of the variables but only $E_3(|\vec{k}_3|^2)$ is dependent on the angles. By integrating over an angle, the derivation is simpler. We can integrate θ_1 relative to any direction and we choose that direction to be $\vec{k}_2-\vec{k}_0$, as shown in Fig. 12.

Since the delta function is not explicitly defined in terms of θ_1 we must make a change in variables, using the identity

$$\delta[g(\theta)] = \sum \frac{\delta(\theta-a)}{|g'(a)|}, \tag{A1}$$

where the sum is over all values of a such that the argument of the delta function is zero and the derivative with respect to θ_1 of the argument of the delta function is not zero.

Then, with $E(|\vec{k}_3|^2)$ written out explicitly in terms of θ_1,

$$g(\theta_1) = E_0 + E_3[|\vec{k}_2-\vec{k}_0|^2 + k_1^2 + 2|k_1||\vec{k}_2-\vec{k}_0|\cos(\theta_1)] - E_1 - E_2. \tag{A2}$$

Using the chain rule for differentiation, we then have

$$|g'(\theta_1)| = \frac{\partial E_3}{\partial(k_3^2)} 2|k_1||\vec{k}_2-\vec{k}_0|\sin(\theta_1). \tag{A3}$$

For polaritons, the expression for $\partial E/\partial(k^2)$ is reasonably compact and easier to derive than $\partial E/\partial k$. For the standard polariton mixing,[9] it is given by

$$\frac{\partial E}{\partial(k^2)} = \frac{\hbar^2\left[\frac{E_{xk}}{m}(E_{ck}^2-E_k^2)+\frac{c^2}{n^2}(E_{xk}^2-E_k^2)\right]}{2E_k[E_{xk}^2+E_{ck}^2+(2\hbar\Omega_R)^2-2E_k^2]}, \tag{A4}$$

where E_k refers to the polariton and E_{ck} and E_{xk} refer to the uncoupled cavity and uncoupled exciton modes, respectively, m is the excitonic mass, n is the effective index of refraction in the microcavity, and Ω_R is the Rabi frequency of the coupling.

Setting $g(\theta_1)=0$ and deriving the values of a by solving for θ_1 results in

$$\delta(\theta_1 - a) \Rightarrow a = \cos^{-1}\left[\frac{k^2(E_3) - |\vec{k}_2 - \vec{k}_0|^2 - |k_1|^2}{2|k_1||\vec{k}_2 - \vec{k}_0|}\right], \tag{A5}$$

where $k^2(E_3)$ corresponds to energy $E_3=E_1+E_2-E_0$. We will write $k(E_3)$ as k_3 from now on.

The argument of the inverse cosine function must be less than 1 and greater than −1. Each of these limits is taken separately after replacing $|\vec{k}_2-\vec{k}_0|^2$ with $|\vec{k}_2|^2+|\vec{k}_0|^2-2|\vec{k}_2||\vec{k}_0|\cos\theta_2$, where θ_2 is measured relative to θ_0. We solve the resulting two equations for the limits of integration over θ_2 and obtain

$$\theta_{2\,min} = \cos^{-1}\left[\frac{k_0^2 - k_1^2 + k_1 k_3}{k_0 k_2}\right], \tag{A6}$$

$$\theta_{2\,max} = \cos^{-1}\left[\frac{k_0^2 - k_1^2 - k_1 k_3}{k_0 k_2}\right]. \tag{A7}$$

Using the relationship $\sin[\cos^{-1}(m)]=[1-m^2]^{1/2}$, we find

$$|g'(\theta_1)| = \frac{\partial E_3}{\partial(k_3^2)} 2|k_1||\vec{k}_2 - \vec{k}_0| \times\left(1 - \left[\frac{k^2(E_3) - |\vec{k}_2 - \vec{k}_0|^2 - |k_1|^2}{2|k_1||\vec{k}_2 - \vec{k}_0|}\right]^2\right)^{1/2}. \tag{A8}$$

Substituting this result and replacing $d^2\vec{k}$ with $kdkd\theta$ in Eq. (9), and integrating over θ_1 gives

$$\frac{\partial n(E_0)}{\partial t} = \frac{S^2 D(E_0)}{(2\pi)^3\hbar} dE_0 \int k_1 dk_1 k_2 dk_2 d\theta_2 \left[\frac{\partial E_3}{\partial(k_3^2)}\right]^{-1} \times \frac{|M(|\vec{k}-\vec{k}_2|)|^2 f(E_0) f(E_3)[1+f(E_1)][1+f(E_2)]}{2|k_1||\vec{k}_2 - \vec{k}|\left\{1 - \left[\frac{k^2(E_3) - |\vec{k}_2 - \vec{k}|^2 - |k_1|^2}{2|k_1||\vec{k}_2 - \vec{k}|}\right]^2\right\}^{1/2}}. \tag{A9}$$

This is converted to an integral over energy using

$$dk = \frac{dE}{\frac{\partial E}{\partial(k^2)} 2k}. \tag{A10}$$

We obtain

$$\frac{\partial n(E_0)}{\partial t} = \frac{S^2 D(E_0)}{4(2\pi)^3\hbar} dE_0 \int dE_1 dE_2 d\theta_2 \times \left[\frac{\partial E_1}{\partial(k_1^2)}\frac{\partial E_2}{\partial(k_2^2)}\frac{\partial E_3}{\partial(k_3^2)}\right]^{-1} \frac{|M(|\vec{k}-\vec{k}_2|)|^2}{2|\vec{k}_1||\vec{k}_2 - \vec{k}_0|} \times \frac{f(E_0) f(E_3)[1+f(E_1)][1+f(E_2)]}{\left\{1 - \left[\frac{k^2(E_3) - |\vec{k}_2 - \vec{k}_0|^2 - |k_1|^2}{2|k_1||\vec{k}_2 - \vec{k}_0|}\right]^2\right\}^{1/2}}. \tag{A11}$$

The denominator can be simplified to give

$$\frac{\partial n(E_0)}{\partial t} = \frac{S^2 D(E_0)}{8(2\pi)^3\hbar} dE \int dE_1 dE_2 d\theta_2 \times \left[\frac{\partial E_1}{\partial(k_1^2)}\frac{\partial E_2}{\partial(k_2^2)}\frac{\partial E_3}{\partial(k_3^2)}\right]^{-1} \frac{|M(|\vec{k}-\vec{k}_2|)|^2}{2|\vec{k}_0||\vec{k}_2|} \times \frac{f(E_0) f(E_3)[1+f(E_1)][1+f(E_2)]}{([\cos(\theta_{2\,min}) - \cos(\theta_2)][(\cos(\theta_2) - \cos(\theta_{2\,max})])^{1/2}}, \tag{A12}$$

where $\theta_{2\,min}$ and $\theta_{2\,max}$ are given in Eqs. (A6) and (A7).

APPENDIX B: PHONON-EMISSION ANGLE INTEGRALS

Changing the sums in Eq. (15) to integrals gives

$$\frac{\partial n_{\vec{k}}}{\partial t} = \frac{1}{\rho u 8\pi^2} \int d^2\vec{k}_1 dq_z X^2_{k,k_1}(q_\parallel^2 + q_z^2)^{1/2} \times\{a_e I_e^{\parallel}[(|\vec{q}|) I_e^{\perp}(q_z) - a_h I_h^{\parallel}(|\vec{q}|) I_h^{\perp}(q_z)]^2 \times n_{\vec{k}}[1+n_{\vec{k}_1}][1+n_{\vec{q}}]\delta[E(\vec{k}) - E(\vec{q}) - E(\vec{k}_1)]. \tag{B1}$$

We replace $d^2\vec{k}_1$ with $k_1 dk_1 d\theta_1$, and assume the system is isotropic in k space, as we did for the polariton-polariton scattering. Therefore, the change to the number of particles within dE of energy E per unit time is

$$\frac{\partial n(E)}{\partial t} = \frac{D(E)}{\rho u 8\pi^2} dE \int k_1 dk_1 d\theta_1 dq_z X^2_{k,k_1}(q_\parallel^2 + q_z^2)^{1/2} \times [a_e I_e^{\parallel}[(|\vec{q}|) I_e^{\perp}(q_z) - a_h I_h^{\parallel}(|\vec{q}|) I_h^{\perp}(q_z)]^2 \times f(E)[1+f(E_1)][1+F(\hbar u|\vec{q}|)] \times \delta(E - \hbar u|\vec{q}| - E_1). \tag{B2}$$

Here, $F(q)$ is the Planck's distribution for phonons.

Instead of integrating out the delta function by integrating over an angle, we integrate over q_z. We again make use of Eq. (A1) and use the form

$$\delta[g(q_z)] = \sum \frac{\delta(q_z - a)}{|g'(a)|} \tag{B3}$$

so that

$$g(q_z) = E - E_1 - \hbar u\sqrt{(|q_\parallel|^2 + q_z^2)} \tag{B4}$$

and

$$|g'(q_z)| = \frac{\hbar u q_z}{\sqrt{(|q_\parallel|^2 + q_z^2)}}. \tag{B5}$$

We set $g(q_z)=0$ and derive the values of a by solving for q_z. The result is

$$a = \left[\frac{(E-E_1)^2}{(\hbar u)^2} - q_\parallel^2\right]^{1/2}. \tag{B6}$$

We now obtain

$$|g'(a)| = \frac{(\hbar u)^2\left[\frac{(E-E_1)^2}{(\hbar u)^2} - |\vec{k}-\vec{k}_1|^2\right]^{1/2}}{E-E_1}. \tag{B7}$$

This derivative cannot equal zero and must be real, so we write

$$\frac{(E-E_1)^2}{(\hbar u)^2} - |\vec{k}-\vec{k}_1|^2 > 0. \tag{B8}$$

Physically, this means that the created phonon has some momentum in the z direction. The elastic wave propagates in both the positive and negative z directions. Since $|\vec{k}-\vec{k}_1|^2 = |\vec{k}|^2 + |\vec{k}_1|^2 - 2|\vec{k}||\vec{k}_1|\cos\theta_1$, we make this substitution and solve for $\cos\theta_1$,

$$\cos\theta_1 = \left[\frac{k^2 + k_1^2 - \frac{(E-E_1)^2}{\hbar^2 u^2}}{2kk_1}\right] < 1. \tag{B9}$$

In the denominator of $g'(a)$, $E \neq E_1$ since if the two energies were the same there would not be a phonon created. Using these results in Eq. (B2) and integrating over q_z gives

$$\begin{aligned}\frac{\partial n(E)}{\partial t} = {} & \frac{D(E)}{\rho u 8\pi^2} dE \int k_1 dk_1 d\theta_1 \\ & \times \frac{X_{k,k_1}(E-E_1)^2}{(\hbar u)^3\left[\frac{(E-E_1)^2}{(\hbar u)^2} - |\vec{k}-\vec{k}_1|^2\right]^{1/2}} \\ & \times [a_e I_e^{\parallel}[(|\vec{q}|)I_e^{\perp}(a) - a_h I_h^{\parallel}(|\vec{q}|)I_h^{\perp}(a)]^2 \\ & \times f(E)[1+f(E_1)][1+F(E-E_1)].\end{aligned} \tag{B10}$$

Converting to integrate over energy, we get

$$\begin{aligned}\frac{\partial n(E)}{\partial t} = {} & \frac{D(E)}{\rho u 16\pi^2} dE \int \frac{dE_1 d\theta_1}{\frac{\partial E_1}{\partial (k_1^2)}} \frac{X_{k,k_1}^2 (E-E_1)^2}{(\hbar u)^3} \\ & \times \left[\frac{(E-E_1)^2}{(\hbar u)^2} - |\vec{k}-\vec{k}_1|^2\right]^{1/2} [a_e I_e^{\parallel}[(|\vec{q}|)I_e^{\perp}(a) \\ & - a_h I_h^{\parallel}(|\vec{q}|)I_h^{\perp}(a)]^2 f(E)[1+f(E_1)][1+F(E-E_1)].\end{aligned} \tag{B11}$$

*Present address: L-3 Corporation Brashear, 615 Epsilon Drive, Pittsburgh, PA 15238.

[1] H. Deng, G. Weihs, D. Snoke, J. Bloch, and Y. Yamamoto, Proc. Natl. Acad. Sci. U.S.A. **100**, 15318 (2003).
[2] J. Kasprzak, M. Richard, S. Kundermann, A. Baas, P. Jeambrun, J. M. J. Keeling, F. M. Marchetti, M. H. Szymańska, R. André, J. L. Staehli, V. Savona, P. B. Littlewood, B. Deveaud, and L. S. Dang, Nature (London) **443**, 409 (2006).
[3] R. Balili, V. Hartwell, D. Snoke, L. Pfeiffer, and K. West, Science **316**, 1007 (2007).
[4] E. Wertz, L. Ferrier, D. D. Solnyshkov, P. Senellart, D. Bajoni, A. Miard, A. Lemaitre, G. Malpuech, and J. Bloch, Appl. Phys. Lett. **95**, 051108 (2009).
[5] A. P. D. Love, D. N. Krizhanovskii, D. M. Whittaker, R. Bouchekioua, D. Sanvitto, S. Al Rizeiqi, R. Bradley, M. S. Skolnick, P. R. Eastham, R. André, and Le Si Dang, Phys. Rev. Lett. **101**, 067404 (2008).
[6] J. J. Baumberg, A. V. Kavokin, S. Christopoulos, A. J. D. Grundy, R. Butté, G. Christmann, D. D. Solnyshkov, G. Malpuech, G. Baldassarri Höger von Högersthal, E. Feltin, J.-F. Carlin, and N. Grandjean, Phys. Rev. Lett. **101**, 136409 (2008).
[7] K. Lagoudakis, M. Wouters, M. Richard, A. Baas, I. Carusotto, R. André, L. S. Dang, and B. Deveaud-Plédran, Nat. Phys. **4**, 706 (2008).
[8] A. Amo, D. Sanvitto, F. P. Laussy, D. Ballarini, E. del Valle, M. D. Martin, A. Lemaitre, J. Bloch, D. N. Krizhanovskii, M. S. Skolnick, C. Tejedor, and L. Viña, Nature (London) **457**, 291 (2009).
[9] A. Kavokin and G. Malpuech, *Cavity Polaritons* (Elsevier, Amsterdam, 2003).
[10] D. W. Snoke and P. B. Littlewood, Phys. Today **63** (8), 42 (2010).
[11] R. Balili, B. Nelsen, D. W. Snoke, L. Pfeiffer, and K. West, Phys. Rev. B **79**, 075319 (2009).
[12] See, e.g., M. H. Szymanska and P. B. Littlewood, Solid State Commun. **124**, 103 (2002).
[13] D. W. Snoke, *Solid State Physics: Essential Concepts* (Pearson/Addison-Wesley, San Francisco, 2009).
[14] D. W. Snoke and J. P. Wolfe, Phys. Rev. B **39**, 4030 (1989).
[15] D. W. Snoke, D. Braun, and M. Cardona, Phys. Rev. B **44**, 2991 (1991).
[16] S. A. Moskalenko and D. W. Snoke, *Bose-Einstein Condensation of Excitons and Biexcitons and Coherent Nonlinear Optics with Excitons* (Cambridge University Press, Cambridge, England, 2000).
[17] D. W. Snoke, Phys. Rev. B **50**, 11583 (1994).
[18] F. Tassone, C. Piermarocchi, V. Savona, A. Quattropani, and P. Schwendimann, Phys. Rev. B **53**, R7642 (1996).
[19] M. Perrin, P. Senellart, A. Lemaitre, and J. Bloch, Phys. Status Solidi C **2**, 3916 (2005).
[20] For example, F. Askary and P. Y. Yu, Phys. Rev. B **31**, 6643 (1985).

[21] F. Tassone, C. Piermarocchi, V. Savona, A. Quattropani, and P. Schwendimann, Phys. Rev. B **56**, 7554 (1997).
[22] F. Tassone and Y. Yamamoto, Phys. Rev. B **59**, 10830 (1999).
[23] G. Rochat, C. Ciuti, V. Savona, C. Piermarocchi, A. Quattropani, and P. Schwendimann, Phys. Rev. B **61**, 13856 (2000).
[24] J. Inoue, T. Brandes, and A. Shimizu, Phys. Rev. B **61**, 2863 (2000).
[25] J. Shumway and D. M. Ceperley, Phys. Rev. B **63**, 165209 (2001).
[26] S. B. de-Leon and B. Laikhtman, Phys. Rev. B **63**, 125306 (2001).
[27] Z. Vörös, D. W. Snoke, L. Pfeiffer, and K. West, Phys. Rev. Lett. **103**, 016403 (2009).
[28] C. Schindler and R. Zimmermann, Phys. Rev. B **78**, 045313 (2008).
[29] G. Malpuech, Y. Rubo, F. Laussy, P. Bigenwald, and A. Kavokin, Semicond. Sci. Technol. **18**, S395 (2003).
[30] R. Rapaport, R. Harel, E. Cohen, A. Ron, E. Linder, and L. N. Pfeiffer, Phys. Rev. Lett. **84**, 1607 (2000).
[31] I. Galbraith and S. Koch, J. Cryst. Growth **159**, 667 (1996).
[32] F. P. Laussy, G. Malpuech, A. Kavokin, and P. Bigenwald, Phys. Rev. Lett. **93**, 016402 (2004).
[33] T. D. Doan and D. B. Tran Thoai, Solid State Commun. **123**, 427 (2002).
[34] H. T. Cao, T. D. Doan, D. B. Tran Thoai, and H. Haug, Phys. Rev. B **69**, 245325 (2004).
[35] T. D. Doan, H. T. Cao, D. B. Tran Thoai, and H. Haug, Phys. Rev. B **72**, 085301 (2005).
[36] T. D. Doan, H. T. Cao, D. B. Tran Thoai, and H. Haug, Phys. Rev. B **74**, 115316 (2006).
[37] D. Porras, C. Ciuti, J. J. Baumberg, and C. Tejedor, Phys. Rev. B **66**, 085304 (2002).
[38] F. Chaves and F. Rodriques, Solid State Commun. **136**, 484 (2005).
[39] D. Sarchi and V. Savona, Phys. Rev. B **75**, 115326 (2007).
[40] D. Sarchi and V. Savona, Solid State Commun. **144**, 371 (2007).
[41] Y. Castin and R. Dum, Phys. Rev. A **57**, 3008 (1998).
[42] C. W. Gardiner and P. Zoller, Phys. Rev. A **58**, 536 (1998).
[43] L. C. Andreani and A. Pasquarello, Phys. Rev. B **42**, 8928 (1990).
[44] S. Adachi, *GaAs and Related Materials: Bulk Semiconducting and Superlattice Properties* (World Scientific, Singapore, 1994).
[45] C. Wolfe, G. Stilman, and W. Lindley, J. Appl. Phys. **41**, 3088 (1970).
[46] C. Piermarocchi, F. Tassone, V. Savona, A. Quattropani, and P. Schwendimann, Phys. Rev. B **53**, 15834 (1996).
[47] G. Arlt and P. Quadflieg, Phys. Status Solidi **25**, 323 (1968).
[48] M. Combescot and O. Betbeder-Matibet, Phys. Rev. B **78**, 125206 (2008).
[49] M. Combescot and D. W. Snoke, Phys. Rev. B **78**, 144303 (2008), and references therein.
[50] W. Press, B. Flannery, S. Teukolsky, and W. Vetterling, *Numerical Recipes in C: The Art of Scientific Computing*, 2nd ed. (Press Syndicate of the University of Cambridge, Cambridge, England, 1992).
[51] C. Ciuti, V. Savona, C. Piermarocchi, A. Quattropani, and P. Schwendimann, Phys. Rev. B **58**, 7926 (1998).
[52] G. Bastard and J. Brum, IEEE J. Quantum Electron. **22**, 1625 (1986).
[53] S. Pau, G. Bjork, J. Jacobson, H. Cao, and Y. Yamamoto, Phys. Rev. B **51**, 7090 (1995).
[54] G. Pikkus and G. Bir, Fiz. Tverd. Tela (Leningrad) **1**, 1642 (1959).
[55] G. Malpuech, A. Kavokin, A. Di Carlo, and J. J. Baumberg, Phys. Rev. B **65**, 153310 (2002).
[56] J. Kasprzak, D. D. Solnyshkov, R. André, L. S. Dang, and G. Malpuech, Phys. Rev. Lett. **101**, 146404 (2008).
[57] M. Perrin, P. Senellart, A. Lemaitre, and J. Bloch, Phys. Rev. B **72**, 075340 (2005).
[58] O. Ambacher, J. Smart, J. Shealy, N. Weinmann, K. Chu, M. Murphy, W. Schaff, and L. Eastman, J. Appl. Phys. **85**, 3222 (1999).
[59] R. Balili, B. Nelsen, D. W. Snoke, R. H. Reid, L. Pfeiffer, and K. West, Phys. Rev. B **81**, 125311 (2010).
[60] K. Hübner, Phys. Status Solidi B **57**, 627 (1973).
[61] M. H. Szymanska, J. Keeling, and P. B. Littlewood, Phys. Rev. Lett. **96**, 230602 (2006).
[62] D. Sarchi and V. Savona, Phys. Status Solidi B **243**, 2317 (2006).
[63] T. Doan, H. T. Cao, D. T. Thoai, and H. Haug, Solid State Commun. **144**, 359 (2007).